Title

Theory of Current Transients in Planar Semiconductor Devices: Insights and Applications to Organic Solar Cells

Journal

Physical Review Applied, 3(4)

ISSN

2331-7043

Authors

Hawks, Steven A
Finck, Benjamin Y
Schwartz, Benjamin J

Publication Date

2015-04-01

DOI

10.1103/physrevapplied.3.044014

Peer reviewed

Theory of Current Transients in Planar Semiconductor Devices: Insights and Applications to Organic Solar Cells

Steven A. Hawks*

Department of Materials Science and Engineering, University of California, Los Angeles, Los Angeles, California 90095, USA

Benjamin Y. Finck and Benjamin J. Schwartz†

Department of Chemistry and Biochemistry, University of California, Los Angeles, Los Angeles, California 90095, USA

(Received 19 December 2014; revised manuscript received 6 March 2015; published 23 April 2015)

Time-domain current measurements are widely used to characterize semiconductor material properties, such as carrier mobility, doping concentration, carrier lifetime, and the static dielectric constant. It is therefore critical that these measurements be theoretically understood if they are to be successfully applied to assess the properties of materials and devices. In this paper, we derive generalized relations for describing current-density transients in planar semiconductor devices at uniform temperature. By spatially averaging the charge densities inside the semiconductor, we are able to provide a rigorous, straightforward, and experimentally relevant way to interpret these measurements. The formalism details several subtle aspects of current transients, including how the electrode charge relates to applied bias and internal space charge, how the displacement current can alter the apparent free-carrier current, and how to understand the integral of a charge-extraction transient. We also demonstrate how the formalism can be employed to derive the current transients arising from simple physical models, like those used to describe charge extraction by linearly increasing voltage (CELIV) and time-of-flight experiments. In doing so, we find that there is a nonintuitive factor-of-2 reduction in the apparent free-carrier concentration that can be easily missed, for example, in the application of charge-extraction models. Finally, to validate our theory and better understand the different current contributions, we perform a full time-domain drift-diffusion simulation of a CELIV trace and compare the results to our formalism. As expected, our analytic equations match precisely with the numerical solutions to the drift-diffusion, Poisson, and continuity equations. Thus, overall, our formalism provides a straightforward and general way to think about how the internal space-charge distribution, the electrode charge, and the externally applied bias translate into a measured current transient in a planar semiconductor device.

DOI: 10.1103/PhysRevApplied.3.044014

I. INTRODUCTION

Planar semiconductor diodes form the backbone of important technologies such as solid-state lighting and photovoltaic energy conversion. The relatively simple physics associated with these one-dimensional devices also makes them ideal for studying the properties of emerging functional materials [1–8]. For instance, in the fields of dye-sensitized solar cells and organic photovoltaics (OPVs) [2,9,10], substantial insights on recombination and charge transport are gained by examining photocurrent, photovoltage, and charge-extraction transients of planar diode devices [11–25]. In terms of specific analysis, examination of the temporal decay of photocurrent transients has been used to measure the charge-transport properties of organic semiconductors [26–28], while the integral of these transients has been taken to quantify initial amounts of photogenerated charge [29–31]. Additionally, charge-extraction transients are routinely used to probe semiconductor recombination kinetics, average doping densities, and carrier mobilities [32–37].

Despite these and countless other studies, the physics of current transients in planar optoelectronic devices is often overlooked or presumed to be obvious. Because such measurements are ultimately a major determinant of benchmark material properties, it is especially important that their physics be thoroughly understood both conceptually and analytically. Thus, in this paper, we present a thorough analytical analysis of current transients in planar diodelike semiconductor devices. Although our reference point comes from the field of OPVs, the equations we present are general and apply to any planar semiconductor device.

Our approach is based on a consideration of the average charge densities within the semiconductor layer. Although

*sahawks@ucla.edu
†schwartz@chem.ucla.edu

some information is lost by averaging, this tactic is not particularly restrictive because, experimentally, one often only has access to spatially averaged values of the carrier concentrations. After deriving an expression for the total measured current, we then present equations describing the subtle but highly important charge on the electrodes as well as the time integral of a current-density transient for the purpose of assessing the initial amount of free charge in the active layer. We find that nonintuitive displacement current effects can easily lead to misinterpretations of charge-extraction measurements.

As examples, we apply our formalism to a variety of transient current experiments commonly used to characterize the active layers of semiconductor diodes, including time-of-flight (TOF) [38,39], transient photocurrent [26,27,40–42], and photoinduced charge extraction by linearly increasing voltage (photo-CELIV) measurements [43–46]. In the context of the original CELIV framework, our generalized formalism reveals a common misinterpretation of CELIV integrals that results in an error in the estimation of the initial free-carrier concentration by at least a factor of 2 [44,47,48]. The existence of such misunderstandings and their increasing prevalence in solar-cell research underlines the importance of the general framework described in this work.

Finally, in order to visualize our formalism and verify that it is built into common drift-diffusion solvers, we numerically simulate a photo-CELIV trace and compare the total current calculated to that predicted by our analytic equations. As expected, the two approaches yield an identical result to within numerical precision, confirming that our formalism is a simple, physically correct, and general way to think about current transients in planar devices.

II. DERIVATION OF A GENERAL CURRENT-DENSITY EQUATION FOR 1D PLANAR SEMICONDUCTOR DIODES

A. Contributions to the total measured current

To analytically analyze current transients in semiconductor devices, we begin by considering a planar diode structure at uniform temperature that is well-described by simple 1D electrodynamics. The relevant equations for the electric current are therefore

$$\frac{dn}{dt} = G - R + G_e^D - R_e^D + G_e^A - R_e^A + \frac{1}{q}\frac{dJ_n}{dx}, \quad (1)$$

$$\frac{dp}{dt} = G - R + G_h^D - R_h^D + G_h^A - R_h^A - \frac{1}{q}\frac{dJ_p}{dx}, \quad (2)$$

$$J_D = \epsilon\frac{dE}{dt}, \quad (3)$$

$$J_{\text{tot}} = J_n + J_p + J_D, \quad (4)$$

where n, p are the mobile-electron and hole concentrations, respectively, G is the generation rate of mobile-carrier pairs, R is the recombination rate of mobile-carrier pairs, $G_{e,h}^{D,A}$ are the generation rates of mobile carriers from localized donor- and acceptor-type trap sites, $R_{e,h}^{D,A}$ are the recombination rates of mobile charge into localized donor- and acceptor-type trap sites, E is the electric field, ϵ is the semiconductor permittivity, q is the absolute value of the electron charge, $J_{n,p}$ are the electric current due to mobile electrons and holes, J_D is Maxwell's displacement current, and J_{tot} is the experimentally measured total electric current at a given time and position in the device. Physically, Eqs. (1) and (2) account for the continuity of mobile carriers and simply add or subtract the contributions of both bulk and trap-mediated recombination or generation to the free-carrier populations.

Our goal is to use the above equations as a starting point to obtain a more insightful and experimentally relevant expression for J_{tot} [Eq. (4)] in terms of the average generation and recombination processes and the average carrier concentrations. In this regard, it is highly important to note that J_{tot} does not vary spatially within the device [see the Supplemental Material (SM) [49] for derivation], which means that the (average) total current anywhere within the active layer is equal to the total current everywhere at a given time.

Our sign convention is chosen such that recombination current is positive and generation current is negative, as is commonly used when reporting experimental (photo)diode currents. Furthermore, it is important to distinguish between the generation and recombination of mobile-carrier pairs (G, R), which are shared terms in the continuity equations, and the individual generation and recombination rates of mobile carriers through immobile trap sites ($G_{e,h}^{D,A}$, $R_{e,h}^{D,A}$), which are not shared because an oppositely charged mobile carrier is not necessarily created or destroyed simultaneously. Traditionally, the $G_{e,h}^{D,A} - R_{e,h}^{D,A}$ terms in Eqs. (1) and (2) are treated as a net recombination rate within the Shockley-Read-Hall formalism [50,51], but such a treatment is not necessary for the derivation at hand.

B. Mobile-carrier currents

To develop a new expression for J_{tot}, we start by integrating Eqs. (1) and (2) across the device thickness to spatially average the continuity equations,

$$J_n(d) = qd\frac{d\bar{n}}{dt} - qd\langle G - R\rangle - qd(\langle G_e^D - R_e^D\rangle + \langle G_e^A - R_e^A\rangle) + J_n(0), \quad (5)$$

$$J_p(0) = qd\frac{d\bar{p}}{dt} - qd\langle G - R\rangle - qd(\langle G_h^D - R_h^D\rangle + \langle G_h^A - R_h^A\rangle) + J_p(d), \quad (6)$$

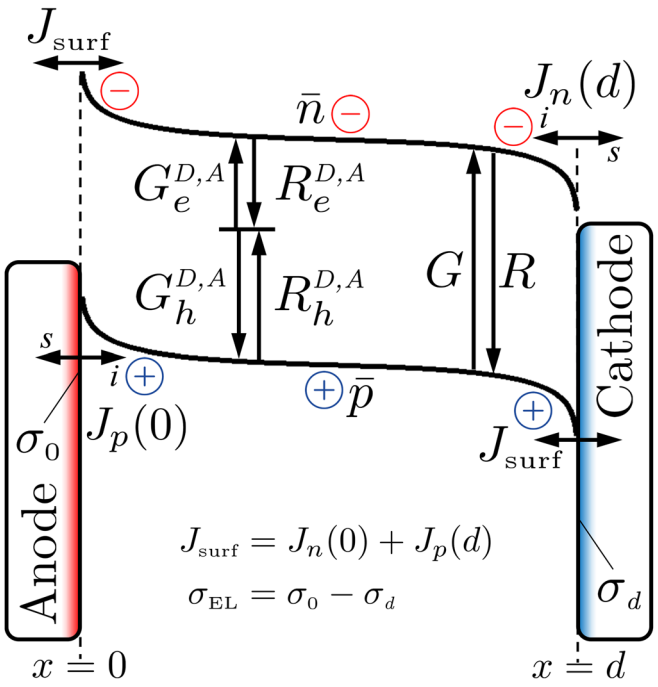

FIG. 1. A schematic band diagram illustrating the device model used in this derivation in forward (positive) bias. The semiconductor (photoactive) layer is sandwiched between metal contacts at $x = 0$ and $x = d$. The i and s scripts on the J_n (electron current) and J_p (hole current) arrows stand for injection and sweep-out, respectively. The average carrier densities are $\bar{n}$ for electrons and $\bar{p}$ for holes. The generation and recombination rates of electron-hole pairs, G and R, are distinct from the rates of freeing and trapping carriers from traps, $G_{e,h}^{D,A}$ and $R_{e,h}^{D,A}$. J_{surf} takes into account the surface current that does not effectively make a transition through the semiconductor energy gap. Note that only the relative heights of the anode and cathode depictions are meant to be part of the implicit energy scale.

where $\bar{n}d = \int_0^d n(x)dx$ and $\bar{p}d = \int_0^d p(x)dx$ are the average carrier concentrations in the active layer, d is the semiconductor active-layer thickness, q is the elementary charge, and $\langle G - R \rangle$ and $\langle G_{e,h}^{D,A} - R_{e,h}^{D,A} \rangle$ are the spatially averaged differences in generation and recombination over the entire active-layer thickness. Figure 1 schematically illustrates the formalism described above on a semiconductor energy-band diagram. Equations (5) and (6) have the advantage of removing the spatial derivative of the free-carrier current densities and replacing them with the averaged quantities and processes of interest. The fact that the current densities are evaluated at the contacts is acceptable because the quantity of interest, J_{tot}, is constant at all positions throughout the active layer.

C. The displacement current

In order to complete the expression for J_{tot} [Eq. (4)], we must also derive expressions for the displacement current J_D [Eq. (3)] at either of the contacts ($x = 0$ and/or d) that are decoupled from each other. We note that simply integrating Gauss's law, $dE/dx = \rho/\epsilon$, and combining with the displacement current [Eq. (3)] will not suffice because $J_D(0)$ and $J_D(d)$ would be coupled. To ultimately decouple $J_D(0)$ and $J_D(d)$, we must use the general 1D solution of Gauss's law for a plane of charge [52] and include the electrode charge in order to relate the electric field at the contacts to the average carrier concentrations within the active layer,

$$E(0) = -\frac{qd}{2\epsilon}(\bar{p} - \bar{n} + \bar{N}_D^+ - \bar{N}_A^-) + \frac{\sigma_{EL}}{2\epsilon}, \tag{7}$$

$$E(d) = \frac{qd}{2\epsilon}(\bar{p} - \bar{n} + \bar{N}_D^+ - \bar{N}_A^-) + \frac{\sigma_{EL}}{2\epsilon}, \tag{8}$$

where $\bar{N}_{D,A}^{+,-}$ are the average number density of immobile ionized trap sites within the active layer, which we consider as localized electron states that can either be neutral when filled (N_D) or neutral when empty (N_A), and are only singly charged. We define $\sigma_{EL} = \sigma_0 - \sigma_d$ to represent the areal charge on the metal electrodes, with $\sigma_{0,d}$ being the areal charge densities on the left and right metal contacts, respectively (Fig. 1). The charge densities $\sigma_{0,d}$ can be either positive, negative, or zero, and we use their difference, σ_{EL}, for the rest of the paper because it is directly proportional to the total electric-field contribution from the charge on the metal electrodes. Additional considerations regarding the charge on the electrodes are presented in Sec. II F below and in the Supplemental Material [49]. We note, though, that the electric field at the contacts is dependent only on the average charge within the active layer and not on its specific distribution, which is a unique consequence of the simple physics of charged 1D planes [52]. Equations (7) and (8) are also the origin of the factor of $1/2$ that will carry on throughout this derivation—another consequence of the physics of charged 1D planes [52].

With the primary electric-field contributions in hand, we can now simply apply Eq. (3) to Eqs. (7) and (8) to obtain the decoupled displacement current at each of the contacts,

$$J_D(0) = \frac{qd}{2}\left(\frac{d\bar{n}}{dt} - \frac{d\bar{p}}{dt}\right) + \frac{qd}{2}\left(\frac{d\bar{N}_A^-}{dt} - \frac{d\bar{N}_D^+}{dt}\right) + \frac{1}{2}\frac{d\sigma_{EL}}{dt}, \tag{9}$$

$$J_D(d) = \frac{qd}{2}\left(\frac{d\bar{p}}{dt} - \frac{d\bar{n}}{dt}\right) + \frac{qd}{2}\left(\frac{d\bar{N}_D^+}{dt} - \frac{d\bar{N}_A^-}{dt}\right) + \frac{1}{2}\frac{d\sigma_{EL}}{dt}. \tag{10}$$

As a check of validity, the difference in the displacement current at the two contacts according to Eqs. (9) and (10) is proportional to the time rate of change of the charge density within the semiconductor layer, which is expected from a simple integration of Gauss's law. Just like the electric fields, these simple expressions for the displacement current at the contacts depend only on the average internal

charge density and not on the charge-density profile—a consequence of the simple physics of planar geometries.

We would now like to substitute Eqs. (9) and (10) along with Eqs. (5) and (6) into Eq. (4) in order to obtain the total measured current density (J_{tot}) at the contacts and therefore everywhere. However, in order to simplify the final result, we first derive relationships between $\bar{N}_{D,A}^{+,-}$ and the kinetic processes that connect them, $G_{e,h}^{D,A}$ and $R_{e,h}^{D,A}$. Fortunately, this derivation is done straightforwardly by summing the generation and recombination events that create and annihilate ionized trap sites, leading to the following kinetic equations:

$$\frac{d\bar{N}_D^+}{dt} = \langle G_e^D - R_e^D \rangle + \langle R_h^D - G_h^D \rangle, \tag{11}$$

$$\frac{d\bar{N}_A^-}{dt} = \langle R_e^A - G_e^A \rangle + \langle G_h^A - R_h^A \rangle. \tag{12}$$

As noted above, these equations only consider singly ionized states.

D. The total measured current

We can now combine all of the relevant relations obtained above to produce a more insightful expression for the total measured electric-current density across the device in terms of the averaged quantities of interest. We do so by combining Eqs. (5) and (6) with Eqs. (9)–(12) at each contact to obtain an expression for J_{tot} [Eq. (4)] as a function of time,

$$J_{\text{tot}} = \frac{qd}{2}\left(\frac{d\bar{p}}{dt} + \frac{d\bar{n}}{dt} + \sum \langle R_{e,h}^{D,A} - G_{e,h}^{D,A} \rangle\right) + qd\langle R - G \rangle + \frac{1}{2}\frac{d\sigma_{\text{EL}}}{dt} + J_{\text{surf}}, \tag{13}$$

where the summation term in Eq. (13) covers all subscript combinations displayed in Eqs. (5) and (6), and the other terms are discussed in detail below.

Equation (13) is the first of two primary theoretical results of this paper. Its simple form—only dependent upon average charge densities and kinetic processes—is a direct consequence of the straightforward physics of charged planes. Equation (13) and the preceding analysis provide a simple conceptual framework for generally thinking about current transients in planar devices as well as reveal nontrivial aspects of these measurements, such as the prefactor of $1/2$ in front of the first term. This general but nonintuitive factor is independent of the carrier distributions and spatial generation and recombination profiles and arises from the combination of Gauss's law and the displacement current for planar 1D electrodynamic systems [Eqs. (7)–(10)]. The factor of $1/2$ means that uniformly injecting or extracting only electrons or holes, for example, results in a measured current proportional to just half of the rate of change in average hole concentration. It also means that current measured by vacating traps, like that in thermally stimulated current, deep-level transient spectroscopy, or even charge-extraction experiments is only half due to mobile charge carriers if sweep-out causes negligible changes in the mobile carrier concentrations [30,34,53–57]. Thus, if this factor of $1/2$ that results from displacement current effects is not properly accounted for, the deduced amount of charge extracted in various experiments will be off by at least a factor of 2. Although this reduction may not be a significant correction for many applications, it at least serves as a lesson that the interpretation of current transients is not necessarily trivial.

Despite the fact that the factor of $1/2$ in Eq. (13) is generally ignored, it is clearly necessary from a conceptual standpoint. Consider the case where mobile carriers are photogenerated within the semiconductor layer with negligible recombination, extraction current, leakage current, or changes in the electrode charge. In such a scenario, the spatially integrated generation rate equals the rate of change of the average concentrations of both carriers, $\langle G \rangle = d\bar{n}/dt = d\bar{p}/dt$, and thus in Eq. (13) the measured current sums to zero, which makes intuitive sense because no current should be measured if mobile carriers are generated uniformly in a hypothetical semiconductor device with no built-in potential or recombination. Such a simple situation could not be understood without the factor of $1/2$ in Eq. (13).

It is also worth noting that even if the changes in electrode charge ($d\sigma_{\text{EL}}/dt$), generation, recombination, and leakage current (J_{surf}) are negligible, the average carrier concentrations can still change implicitly by charge-carrier flow through the correct contact (i.e., extraction by sweep-out and filling by injection for a diode; see Fig. 1) [26,58], which are critical aspects of any solar cell or LED. Indeed Eq. (13) could be optionally rewritten as $J_{\text{tot}} = J_{i,s} + J_{\text{EL}} + J_{\text{surf}}$, where $J_{i,s}$ is composed of the first two terms of Eq. (13) and embodies the net injection or sweep-out (extraction) of carriers into or out of the semiconductor material, and J_{EL}, the third term in Eq. (13), represents the current density due to changes in the electrode charge density [see Eq. (15), discussed below], and the last term, J_{surf}, takes into account the surface current that does not effectively make a transition through the semiconductor energy gap.

E. Surface recombination at the wrong contacts

As just alluded to, the J_{surf} term in Eq. (13) accounts for current that effectively traverses the active layer without making a transition through the semiconductor energy gap. Here, J_{surf} is mathematically defined as $J_{\text{surf}} = J_n(0) + J_p(d)$. For a diode, J_{surf} is surface recombination that includes the net electron extraction or injection at the hole-selective contact (anode) and net hole extraction or injection at the electron-selective contact (cathode; see Fig. 1). In other words, herein, positive J_{surf} corresponds to net carrier

extraction at the wrong contact(s) while negative J_{surf} corresponds to net carrier injection at the wrong contact(s). The J_{surf} term is often referred to as shunt or leakage current in diodes, LEDs, and solar cells, and we use all of these terms interchangeably. In addition to Ohmic-like leakage [59], the implied surface recombination that underlies J_{surf} is expected in OPV diodes to have an exponential voltage dependence with low ideality factor and therefore will be important at higher biases or charge densities [60–62]. In single-carrier devices, J_{surf} is often analyzed from the standpoint of space-charge-limited current [63].

F. Areal charge densities on the contacts

A highly important aspect of Eq. (13) is that the seemingly benign $d\sigma_{EL}/dt$ term can often significantly contribute to the total measured current. To better understand this term, here we discuss the physical attributes of the device that determine σ_{EL}.

The free-carrier density of the metal electrodes is typically sufficiently high such that the electric field is zero inside them at all times [64]. Under this reasonable (but not always true [65]) limit, the total areal charge summed over both electrodes must be equal and opposite to the total charge within the active layer, or $\sigma_0 + \sigma_d = -qd(\bar{p} - \bar{n} + \bar{N}_D^+ - \bar{N}_A^-)$. A related consequence is that the surface charge is directly proportional to the electric field immediately outside the surface, or $\sigma_0 = \epsilon E(0)$ and $\sigma_d = -\epsilon E(d)$ [66], where the sign of $\sigma_{0,d}$ depends on the sign of the charge. These relations will be used below in conjunction with drift-diffusion calculations to determine σ_{EL} at various times during a simulated solar cell photo-CELIV transient.

One can conceptually imagine the σ_{EL} term as a variable quantity that is used to supply enough electric field to meet the imposed voltage conditions. As derived in the SM [49], σ_{EL} is only a function of the space-charge distribution within the device and the electric-potential drop across the active layer ($V = -\int_0^d E dx$) according to

$$\sigma_{EL} = \bar{\rho} d - \frac{2}{d}\int_0^d \int_0^x \rho(x')dx'dx - \frac{2\epsilon V}{d}, \quad (14)$$

$$J_{EL} = \frac{d}{2}\frac{d\bar{\rho}}{dt} - \frac{1}{d}\int_0^d \int_0^x \frac{d\rho(x')}{dt}dx'dx - \frac{\epsilon}{d}\frac{dV}{dt}, \quad (15)$$

where $\rho(x) = q[p(x) - n(x) + N_D^+(x) - N_A^-(x)]$, x' is a dummy variable for spatial integration, $2J_{EL} = d\sigma_{EL}/dt$, and $\bar{\rho} d = \int_0^d \rho(x)dx$.

Equations (14) and (15) show that $d\sigma_{EL}/dt$ is nonzero only if the applied bias or the spatial distribution of net charge is changing with time. We strongly emphasize that V in Eq. (14) and all other equations herein is just the electric-potential difference across the active layer and not the total potential difference (V_{tot}). The total potential difference in a diode often includes an additional built-in (diffusion, composition, etc.) potential (V_{BI}) that is nominally constant with light intensity and applied bias [67]. Since V_{BI} is usually well-approximated as a constant, the electric potential and total potential are related by $V(t) = V_{tot}(t) - V_{BI}$, and the conclusions made herein are essentially unchanged.

Equations (14) and (15) also tell us something about the measured device capacitance, as is recognized by the fact that the voltage derivative of Eq. (14) is related to the electrode capacitance, though one must also account for the charge stored in the active layer (chemical capacitance) when considering the total measured capacitance of a diode [68–70]. Interestingly, though, Eq. (15) reduces to the classical parallel-plate capacitor current, $C_g dV/dt$, where $C_g = \epsilon/d$ if the internal space-charge distribution is not changing in time, independent of the space-charge distribution. In other words, Eq. (15) implies that the effective device geometric capacitance is independent of any static space-charge profile, only deviating from its classical value of ϵ/d when the internal space-charge distribution is changing in time. Unfortunately, since the difference in electric potential between the contacts depends on the specific space-charge distribution, it is not possible to determine a simpler relationship between the effective geometric capacitance, the charge on the electrodes, and the potential difference across the device beyond what is presented in Eqs. (14) and (15). Additionally, as an aside, the σ_{EL} term can be eliminated to yield a generalized relation between the electric-field profile $E(x)$, the electric-potential difference across the device V, and the internal space-charge/permittivity profile fraction $\rho(x)/\epsilon(x)$ [see SM [49], Eq. (S12)].

G. Integrating the total measured current

The factor of $1/2$ in Eq. (13) is relevant to experiments on diodes because Eq. (13) is often experimentally integrated over an extraction-current transient in order to estimate the initial average steady-state carrier concentration in such devices [13,16,17,32,71–73]. When integrating Eq. (13) over a current transient and multiplying by $1/qd$, we find that the apparent initial carrier concentration ($\Delta\bar{n}_{meas}$) is

$$\Delta\bar{n}_{meas} = \frac{1}{2}(\Delta\bar{n} + \Delta\bar{p}) + \frac{\Delta\sigma_{EL}}{2qd} + \int_0^{t_f}\left(\frac{J_{surf}}{qd} + \frac{1}{2}\sum\langle R_{e,h}^{D,A} - G_{e,h}^{D,A}\rangle + \langle R - G\rangle\right)dt, \quad (16)$$

where the difference terms are negative for an extraction current transient. These terms are given by, for example, $\Delta\bar{n} = \bar{n}(t_f) - \bar{n}(0)$, evaluated at the start ($t = 0$) and finish ($t = t_f$) of the transient. The left-hand side of Eq. (16) is given by $qd\Delta\bar{n}_{meas} = \int_0^{t_f} J_{tot}(t)dt$ and is the apparent

amount of charge extracted or injected from integration of the (experimental) current transient.

Equation (16) is the other primary theoretical result of this paper because integrated extraction-current transients are widely used, particularly in the organic-solar-cell community, to measure average steady-state carrier concentrations [11,13,15,32,71,74,75]. Equation (16) provides significant physical insight into integrated current transients because it details all of the apparent sources of charge present in a 1D (extraction) current transient [12,73,74]. Notably, the factor of $1/2$ in the first term of Eq. (13) persists, which as we discuss further below, has resulted in errors in the estimation of the average charge density when such experiments were performed on organic-solar-cell devices.

Examples of common methods that rely heavily on integrating current transients include the CELIV [43], charge-extraction [23,32], and time-delayed collection-field techniques [29]. Although these methods allow experimenters to estimate the total average carrier concentrations relative to a short-circuit or quasidepleted state, they have the downside of having to correct for the change in charge on the electrodes ($\Delta\sigma_{\mathrm{EL}}$) at the beginning and end of the transient. Equations (14) and (16) clarify this previously nebulous correction. In particular, Eq. (14) reveals that $\Delta\sigma_{\mathrm{EL}}$ is only a function of the geometric capacitance (C_g), the change in applied bias (ΔV), and the change in the internal charge-density profile [$\Delta\rho(x)$] from the beginning and end of the transient.

In many polymer-fullerene bulk-heterojunction (BHJ) OPVs, researchers have found that consideration of only the voltage conditions and the geometric capacitance [the last term in Eq. (14)] is sufficient to account for $\Delta\sigma_{\mathrm{EL}}$ in their charge-extraction measurements [17,32,72,74,76,77]. The success of this correction implies that the OPV devices in these experiments experienced negligible changes in the internal space-charge distribution between the beginning and ending of the extraction transient. Because most BHJ OPVs are thin, have low dielectric constants, and are weakly or undoped, this observation also suggests that such devices are largely space-charge free over the operational voltage regime (i.e., have a linear band structure). These conclusions, however, are not obvious without the help of Eqs. (14) and (16).

Finally, it is common to approximate the initial amount of photogenerated charge in organic photovoltaic devices by integrating a transient photocurrent taken at a constant dc bias [16,17,72]. This approach typically relies on a quick laser flash to photogenerate a mobile charge, which due to the built-in potential and/or externally applied bias, results in a current transient. This transient is then integrated over time to estimate the initial amount of photogenerated charge. Equation (16) shows that if the bias and light intensity have the same initial and final values, and if generation, recombination, and leakage current can be ignored (or corrected for), then $\Delta\sigma_{\mathrm{EL}} = 0$ and the integral of the photocurrent decay is actually equal to half the sum of the average initial photogenerated charge-carrier densities. Since photogeneration typically gives $\Delta n = \Delta p$, the integral of a photocurrent transient without generation, recombination, or leakage current gives an apparent initial excess carrier concentration of $\Delta\bar{n}_{\mathrm{meas}} = \Delta\bar{n} = \Delta\bar{p}$. We note that these considerations are independent of the generation profile or initial carrier-concentration distributions.

III. ANALYTICAL APPLICATIONS OF THE MODEL: IMPLICATIONS FOR MATERIALS CHARACTERIZATION

A. The time-of-flight experiment

A classic approach to measuring the charge-transport properties of materials is via a time-of-flight (TOF) or transient-photoconductivity experiment [26,27,38–40,78,79]. Although TOF techniques are well documented, discussing the TOF conceptual model in terms of Eqs. (13) and (15) is insightful and illustrative of the different possible sources of current in such measurements or models. We note that we do not consider aspects of trap-limited dispersive transport here, but rather emphasize that the basic physics of such measurements must first be fully understood before new or unique physical effects can be identified. Moreover, this discussion demonstrates how readily a simple physical picture can be translated into a theoretically measured current transient using the equations presented above and in the SM [49].

In the TOF experiment, a planar device is used and the semiconducting material of interest is made thick so that a laser flash photogenerates an approximately planar carrier packet at one side of the device. During the measurement, a constant applied bias and/or built-in potential is used to drive the carrier plane across the sample. Theoretically, in terms of Eqs. (14) and (15), this situation corresponds to a space-charge profile of $\rho(x) = \sigma_{\mathrm{gen}}\delta(x - x_\sigma(t))$, where δ is the Dirac delta function, σ_{gen} is the charge density of the drifting plane, and $x_\sigma(t)$ is the spatial position of the plane of charge. Since $dV/dt = 0$ and V is dependent on $x_\sigma(t)$, a continuous supply of charge must be given to the electrodes in order to keep the voltage constant as the carrier plain drifts across the sample. Thus, by inspection of Eq. (13), the only source of current in the TOF model arises from changes in electrode charge. The current transient is readily derived by substituting $\rho(x) = \sigma_{\mathrm{gen}}\delta(x - x_\sigma(t))$ into Eq. (15),

$$J_{\mathrm{tot}} = J_{\mathrm{EL}} = \frac{\sigma_{\mathrm{gen}}}{d}\frac{dx_\sigma(t)}{dt} = q\bar{p}\mu E_{\mathrm{EL}}, \tag{17}$$

where μ is the mobility of the carrier plane, E_{EL} is the electric field supplied by the electrode charge [see SM [49], Eq. (S10)], and $\bar{p} = \sigma_{\mathrm{gen}}/qd$ is the spatially averaged carrier concentration, assumed here to arise from a plane of positive charge originating at $x = 0$. Since the total current is

rigorously constant everywhere (see the SM [49]), the TOF transient also can be rewritten as just the average drift current flowing within the device [right-hand side of Eq. (17)]. The solution of Eq. (17) can be readily obtained with the aid of Eq. (S10) [49] upon substituting $\rho(x) = \sigma_{\text{gen}}\delta(x - x_\sigma(t))$, giving the following differential equation and subsequent expression for the TOF current transient:

$$\frac{dx_\sigma(t)}{dt} = \mu E_{\text{EL}} = \frac{x_\sigma(t)}{\tau} - \frac{d}{2\tau} - \frac{\mu V}{d}, \tag{18}$$

$$J_{\text{TOF}} = -\left(\frac{qd\bar{p}}{\tau} + \frac{q\bar{p}\mu V}{d}\right)e^{(t/\tau)}, \tag{19}$$

where $\tau = \epsilon/q\bar{p}\mu$ is the dielectric relaxation time of the semiconductor with excess conductive charge $\bar{p}$, V is assumed to be negative, and the carrier plane starts at $x = 0$. Thus, for large values of τ and high magnitudes of V, the value of J_{TOF} is, as expected, approximately constant in time and equal to $q\bar{p}\mu V/d$ due to an approximately constant velocity of the drifting plane of charge.

In short, this derivation demonstrates that Eqs. (13), (14), and (S10) [49] readily capture all the essential features and fine details of the classic TOF experiment, illustrating how a simple physical picture (a plane of charge moving across a device) results in an actual measured current transient [Eq. (19)]. This example also shows how simple current-transient models in planar optoelectronic devices readily fit within the general relations derived in this work.

B. Determination of the average carrier concentration with CELIV

As a more detailed example of the utility of Eqs. (13), (14), and (16) when applied to charge-extraction techniques that vary the applied bias, in this section we reexamine the assumptions underlying the CELIV framework for measuring charge densities in solar-cell devices. The original analytical model describing CELIV transients by Juska *et al.* [43] considered a unipolar device with flat-band contacts and no generation, recombination, or leakage current. This model also ignores diffusion current, considering only a slab of uniform-density charge drifting under the influence of an electric field [Fig. 2(a)]. Lorrmann *et al.* [44] and Sandberg *et al.* [80] later presented an excellent analysis of the mathematical implications of this CELIV model using the same original assumptions and equations as Juska *et al.* [43],

$$J_{\text{tot}} = \frac{U_R\epsilon}{d} + nq\left(1 - \frac{l(t)}{d}\right)\frac{dl(t)}{dt}, \tag{20}$$

$$\frac{dl(t)}{dt} = \frac{\mu U_R t}{d} - \frac{nq\mu}{2\epsilon d}l(t)^2, \tag{21}$$

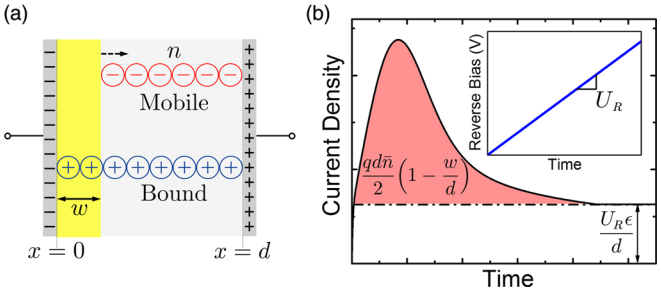

FIG. 2. (a) Schematic representation of the CELIV model device under consideration. A uniform block of free charge with local density n and average density $n(1 - w/d)$ is swept out under a linearly changing reverse bias pulse [inset of (b)]. Here, w denotes the steady-state initial depletion width. (b) An example CELIV current transient showing the typical portion of the curve that is integrated to yield the initial uniform free-carrier density (n). Nonintuitively, the shaded region is at most proportional to half of the initial average free-charge density and even further reduced if w is nonzero.

where U_R is the voltage ramp rate, d the film thickness, n is the uniform unipolar free-carrier density, $l(t)$ is the time-dependent extraction depth (i.e., depletion width), μ is the unipolar carrier mobility, ϵ the semiconductor permittivity, and J_{tot} the total measured current density. The properties of $l(t)$ are: $l(0) = w$, $dl(0)/dt = 0$, $0 \le l(t) \le d$, and $l(t_{\text{tr}}) = d$, where t_{tr} is the time taken to extract all the mobile carriers within the active layer. Schottky junctions under the full-depletion assumption are well approximated by this model through a finite initial steady-state depletion width, w [Fig. 2(a)] [80].

In examining how this model is used in the literature, we find that the integral of Eq. (20) is often misinterpreted because of the factor of $1/2$ in the first terms of Eqs. (13) and (16) due to improper accounting of $\Delta\sigma_{\text{EL}}$. Although this factor of $1/2$ was recently noticed by Sandberg *et al.* [80] for the CELIV model described above, the origin of this term was not discussed. The issue arises from attributing the second term in Eq. (20) solely to mobile carriers [81]. Under this seductive but incorrect assumption, subtracting the time-independent $U_R\epsilon/d$ term and integrating [shaded area in Fig. 2(b)] yields the presumed total number of free carriers extracted and thus the initial carrier density [46,48].

If this incorrect assumption were true, however, then integrating the second term of Eq. (20) from $t = 0$ to t_{tr} and multiplying by $1/qd$ should give the actual initial carrier concentration n. Instead, we find that

$$\bar{n}_{\text{meas,CELIV}} = \frac{n}{d}\int_0^{t_{\text{tr}}}\left(1 - \frac{l(t)}{d}\right)\frac{dl(t)}{dt}dt, \tag{22}$$

$$= \frac{n}{2}\left(1 - \frac{l(0)}{d}\right)^2, \tag{23}$$

$$= \frac{\bar{n}}{2}\left(1 - \frac{w}{d}\right), \tag{24}$$

where $dq\bar{n}_{\mathrm{meas,CELIV}} = \int_0^{t_{\mathrm{tr}}}[J(t) - U_R\epsilon/d]dt$ is the apparent initial carrier concentration in the Juska *et al.* [43] model, obtained by integrating the CELIV transient with $U_R\epsilon/d$ subtracted away and $l(0) = w$ as the initial steady-state depletion width [80]. Thus, we see that integrating a CELIV transient in this model over the total evacuation time t_{tr} gives at most half of the actual mobile charges extracted, which is in exact agreement with Eq. (16) under the same assumptions.

In addition to this factor-of-1/2 reduction, Eq. (24) also shows that there is another reduction of the apparent initial average free-charge density by an additional factor of $1 - w/d$. Inspection of Eq. (16) readily reveals that this reduction is due to electrode-charge effects. Indeed, Eq. (16) indicates that if there is an initial steady-state depletion width, $w > 0$, then the initial charge on the electrodes ($\sigma_{\mathrm{EL}}(t = 0)$) will be finite due to the initial presence of space charge. Thus, the $\Delta\sigma_{\mathrm{EL}}$ correction in Eq. (24) will be altered from the case where $w = 0$, since both cases end in an identical fully depleted state. This additional reduction due to $\Delta\sigma_{\mathrm{EL}}$ is generally nontrivial since in real devices the steady-state space-charge profile can take on shapes more complex than the simple rectangular version assumed by the CELIV model. Overall, though, these previously nebulous aspects of current transients are decoupled and made obvious by Eqs. (13), (14), and (16), thus highlighting the conceptual utility of our formalism. Overall, Eq. (16) readily corrects a common misinterpretation of CELIV transients and explains why, for example, Lorrmann *et al.* [44] concluded that a substantial fraction of the mobile charge within the active layer was not extracted during CELIV, even after long extraction times (~1 ms).

It is worth noting that none of the above analysis includes *RC* time-constant effects [82], which inevitably makes interpretation of the current transients more complicated. However, we find through numerical simulations that when *RC* effects are included at reasonable levels ($\tau_{RC} \approx 300$ ns), the conclusions we reach for low-mobility materials are not altered. Moreover, *RC* effects should mostly influence the temporal shape of the current transient, leaving the integral [Eq. (16)] largely unaffected.

IV. UNDERSTANDING THE FORMALISM VIA TIME-DEPENDENT DRIFT-DIFFUSION MODELING: CELIV REVISITED

Last, to better understand each of the terms underlying the total current in Eq. (13) and the analysis in the previous section, we performed time-dependent drift-diffusion numerical modeling to simulate a photo-CELIV measurement. In the following, we demonstrate that Eq. (13) is compatible with detailed numerical drift-diffusion simulations, verifying that we obtain a physically correct expression for the total current.

TABLE I. Parameters used in the drift-diffusion photo-CELIV simulation; the values chosen are designed to roughly simulate an organic photovoltaic device.

Parameter	Symbol	Value
Electron hole mobility	μ_n, μ_p	1×10^{-4} cm^2/V s
Active layer thickness	d	100 nm
Relative permittivity	ϵ_r	3.5
Injection barriers	ϕ_n, ϕ_p	0.3 eV
Langevin reduction factor	γ	0.1
Built-in voltage	V_{BI}	0.6 V
Effective density of states	N_C, N_V	1×10^{20} cm^{-3}
Temperature	T	298 K
Band gap	E_g	1.2 eV

The drift-diffusion approach involves solving the continuity equations [Eqs. (1) and (2)] along with the Poisson equation to determine the individual carrier concentrations and the electric field during the simulation. To explicitly solve these equations, the approach assumes that the current densities follow the drift-diffusion form,

$$J_n = qn\mu_n E + \mu_n kT\frac{dn}{dx}, \tag{25}$$

$$J_p = qp\mu_p E - \mu_p kT\frac{dp}{dx}, \tag{26}$$

where μ_n and μ_p refer to the mobility of electrons and holes, respectively, and kT is the thermal energy. We have previously performed steady-state drift-diffusion calculations to model OPV devices using homemade code [83], and we employ the same approach here only extended into the time domain (see the SM [49] for a detailed description of our drift-diffusion computational approach). In this study, the time dependence is accounted for by solving the continuity equations and employing an implicit method to iterate forward in time. Recombination is assumed to take the simple reduced Langevin form [$R = q\gamma np(\mu_n + \mu_p)/\epsilon$; see Table I] [28,84,85], and the generation profile is taken from a transfer-matrix calculation using experimentally available optical constants for the different layers [86,87]. The device parameters for our simulations are presented in Table I, and are loosely designed to be nominally representative of those of a polymer-based solar cell using poly(3-hexylthiophene-2,5-diyl) (P3HT) and phenyl–C61–butyric acid methyl ester (PCBM) [83,88]. We choose to simulate an organic-solar-cell photo-CELIV transient because photo-CELIV is a common method for studying low-mobility semiconductors and the technique involves many of the physical processes that our analytical model aims to capture: generation, recombination, and a time-varying applied voltage. The $\langle R_{e,h}^{D,A} - G_{e,h}^{D,A}\rangle$ term is the only term in

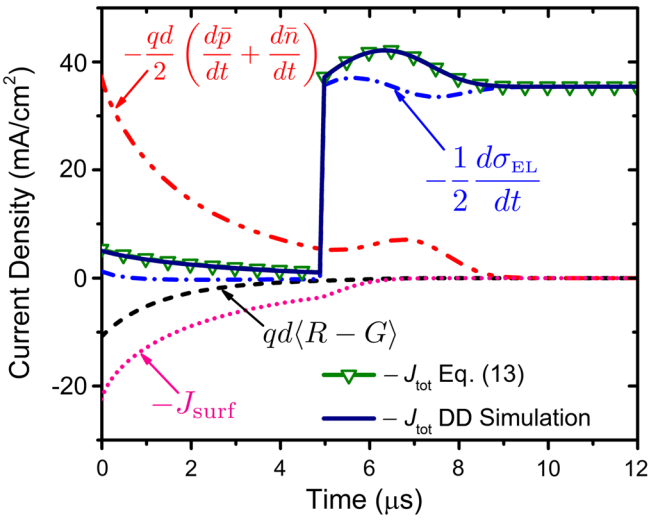

FIG. 3. The various current contributions from Eq. (13) determined from numerical drift-diffusion (DD) simulations and the negative of their sum $-J_{tot}$ (upside down open triangles). Note that here the reverse-bias extraction current is plotted as positive. The simulated CELIV ramp conditions are 0.1 V/μs starting at an initial forward bias of 0.6 V. The total current density from the simulation is also shown (solid blue line, labeled DD Simulation). The simulated total current density and the summed current density from Eq. (13) lie on top of each other, showing their precise quantitative agreement. We note that trapping is not included in the numerical model and thus is assumed to be zero.

Eq. (13) not accounted for in this simulation, and is therefore assumed to be zero.

We simulate the photo-CELIV experiment by first performing a steady-state calculation to verify that the dark J-V characteristics of the device are reasonable. Then, for the transient, our virtual device is initially held in the dark at an applied bias equal to the built-in potential V_{BI} (Table I). Next, these steady-state conditions are perturbed by a brief pulse of illumination to produce excess carriers. After this pulse, the photogeneration of carriers is set to zero and, after an additional short period of time (5 μs), a linear reverse bias voltage ramp is applied to sweep out any remaining photogenerated charge.

To visualize Eq. (13), we explicitly calculate each term during the simulated photo-CELIV process and compare their sum to the total current calculated from the drift-diffusion simulation (Fig. 3). We plot in Fig. 3 the negative of the total current ($-J_{tot}$) calculated by each approach, since $-J_{tot}$ is what is typically reported in the literature for CELIV transients [37,45,89–92]. Because the drift-diffusion simulations use a different starting formalism than Eq. (13), the fact that the two results agree precisely verifies the legitimacy and generality of our derivation. Furthermore, as also highlighted in the TOF section, this agreement shows that Eq. (13) and Eqs. (25) and (26) can be combined to examine the materials-related aspects of these transients.

In addition to the negative of the total current, Fig. 3 also shows the negative of each component of Eq. (13). The current due to the changing electrode charge runs in the opposite direction for this case because CELIV involves a reverse-bias voltage ramp. The carrier concentrations decrease in time due to recombination, sweep-out, and surface recombination current, and therefore the derivative of the average carrier concentrations are also negative. Since generation only takes place initially and is set to zero afterwards, only recombination contributes to the $qd\langle R-G\rangle$ term in Eq. (13), which registers as a positive current density in our sign convention.

Finally, it is worth noting that the J_{surf} term is rather large and positive in the initial part of the transient in Fig. 3, corresponding to net carrier extraction at the wrong contacts. The reason for such a large value of this current density is that the cell is initially held at a forward bias equal to the built-in potential until the start of the CELIV ramp. At this applied bias, the built-in electric field is entirely canceled, and thus a significant amount of excess carriers get collected at the wrong contact by way of diffusion. Real, well-working, devices are designed to avoid this problem by having higher built-in potentials and/or blocking layers to prevent extraction of carriers by the wrong contact.

All in all, Fig. 3 verifies that our formalism provides another level of insight into current-transient measurements that is fully consistent with detailed time-domain numerical drift-diffusion modeling. The benefit of our approach, though, is that it pairs the generality of a full numerical calculation with the physical insight of an analytical model. With these tools at hand, researchers can now understand any current-transient measurement in terms of a simple set of discrete physical processes.

V. CONCLUSIONS

In summary, we derive a generalized equation for describing current transients in planar optoelectronic devices at uniform temperature. Our results detail all the possible sources of current using only fundamental physical equations and spatially averaged values of the quantities or processes of interest. Integrating our generalized current-density equation provides further insight on how to interpret the apparent charge extracted from transient current measurements, including how to account for changes in charge on the electrodes. One unexpected result from this analysis is a factor-of-1/2 reduction in the apparent extracted charge due to nonintuitive displacement current effects. We show how this factor of 1/2, along with an improper accounting of the electrode charge, can easily lead to misinterpretations of charge-extraction transients. We further demonstrate how readily a simple physical picture—like that of the classic CELIV and TOF models—can be translated into an expression for the total measured current density as a function of time using our set of simple

generalized equations. Finally, we show that the derived relations are effectively built into time-domain drift-diffusion numerical solvers, thus verifying the correctness of our approach while demonstrating an alternative avenue for understanding current transients in 1D optoelectronic devices.

ACKNOWLEDGMENTS

The authors acknowledge support from the Molecularly Engineered Energy Materials (MEEM), an Energy Frontier Research Center funded by the U.S. Department of Energy, Office of Science, Office of Basic Energy Sciences under Grant No. DE-SC0001342 and from the National Science Foundation Grant No. CHE-1112569. S. A. H. also acknowledges previous support by the NSF IGERT Materials Creation Training Program No. MCTP-DGE-0654431.

[1] S. M. Sze and K. K. Ng, *Physics of Semiconductor Devices*, 3rd ed. (Wiley-Interscience, Hoboken, NJ, 2007).
[2] C. Deibel and V. Dyakonov, Polymer-fullerene bulk heterojunction solar cells, Rep. Prog. Phys. **73**, 096401 (2010).
[3] G. Dennler, M. C. Scharber, and C. J. Brabec, Polymer-fullerene bulk-heterojunction solar cells, Adv. Mater. **21**, 1323 (2009).
[4] J. Nelson, Polymer:fullerene bulk heterojunction solar cells, Mater. Today **14**, 462 (2011).
[5] H. Snaith, Perovskites: The emergence of a new era for low-cost, high-efficiency solar cells, J. Phys. Chem. Lett. **4**, 3623 (2013).
[6] M. Liu, M. B. Johnston, and H. J. Snaith, Efficient planar heterojunction perovskite solar cells by vapour deposition, Nature (London) **501**, 395 (2013).
[7] A. Mei, X. Li, L. Liu, Z. Ku, T. Liu, Y. Rong, M. Xu, M. Hu, J. Chen, Y. Yang, M. Gratzel, and H. Han, A hole-conductor-free, fully printable mesoscopic perovskite solar cell with high stability, Science **345**, 295 (2014).
[8] M. M. Lee, J. Teuscher, T. Miyasaka, T. N. Murakami, and H. J. Snaith, Efficient hybrid solar cells based on meso-superstructured organometal halide perovskites, Science **338**, 643 (2012).
[9] C. J. Brabec, S. Gowrisanker, J. J. M. Halls, D. Laird, S. Jia, and S. P. Williams, Polymer-fullerene bulk-heterojunction solar cells, Adv. Mater. **22**, 3839 (2010).
[10] C. J. Brabec, M. Heeney, I. McCulloch, and J. Nelson, Influence of blend microstructure on bulk heterojunction organic photovoltaic performance, Chem. Soc. Rev. **40**, 1185 (2011).
[11] C. G. Shuttle, B. O'Regan, A. M. Ballantyne, J. Nelson, D. D. C. Bradley, J. de Mello, and J. R. Durrant, Experimental determination of the rate law for charge carrier decay in a polythiophene:fullerene solar cell, Appl. Phys. Lett. **92**, 093311 (2008).
[12] C. G. Shuttle, R. Hamilton, J. Nelson, B. C. O'Regan, and J. R. Durrant, Measurement of charge-density dependence of carrier mobility in an organic semiconductor blend, Adv. Funct. Mater. **20**, 698 (2010).
[13] A. Maurano, R. Hamilton, C. G. Shuttle, A. M. Ballantyne, J. Nelson, B. O'Regan, W. M. Zhang, I. McCulloch, H. Azimi, M. Morana, C. J. Brabec, and J. R. Durrant, Recombination dynamics as a key determinant of open circuit voltage in organic bulk heterojunction solar cells: A comparison of four different donor polymers, Adv. Mater. **22**, 4987 (2010).
[14] S. A. Hawks, F. Deledalle, J. Yao, D. G. Rebois, G. Li, J. Nelson, Y. Yang, T. Kirchartz, and J. R. Durrant, Relating recombination, density of states, and device performance in an efficient polymer:fullerene organic solar cell blend, Adv. Energy Mater. **3**, 1201 (2013).
[15] R. Hamilton, C. G. Shuttle, B. O'Regan, T. C. Hammant, J. Nelson, and J. R. Durrant, Recombination in annealed and nonannealed polythiophene/fullerene solar cells: Transient photovoltage studies versus numerical modeling, J. Phys. Chem. Lett. **1**, 1432 (2010).
[16] D. Credgington, R. Hamilton, P. Atienzar, J. Nelson, and J. R. Durrant, Non-geminate recombination as the primary determinant of open-circuit voltage in polythiophene: fullerene blend solar cells: An analysis of the influence of device processing conditions, Adv. Funct. Mater. **21**, 2744 (2011).
[17] D. Credgington and J. R. Durrant, Insights from transient optoelectronic analyses on the open-circuit voltage of organic solar cells, J. Phys. Chem. Lett. **3**, 1465 (2012).
[18] F. Deledalle, P. Shakya Tuladhar, J. Nelson, J. R. Durrant, and T. Kirchartz, Understanding the apparent charge density dependence of mobility and lifetime in organic bulk heterojunction solar cells, J. Phys. Chem. C **118**, 8837 (2014).
[19] G. F. A. Dibb, T. Kirchartz, D. Credgington, J. R. Durrant, and J. Nelson, Analysis of the relationship between linearity of corrected photocurrent and the order of recombination in organic solar cells, J. Phys. Chem. Lett. **2**, 2407 (2011).
[20] G. F. A. Dibb, F. C. Jamieson, A. Maurano, J. Nelson, and J. R. Durrant, Limits on the fill factor in organic photovoltaics: Distinguishing nongeminate and geminate recombination mechanisms, J. Phys. Chem. Lett. **4**, 803 (2013).
[21] B. C. O'Regan and F. Lenzmann, Charge transport and recombination in a nanoscale interpenetrating network of *n*-type and *p*-type semiconductors: Transient photocurrent and photovoltage studies of TiO_2/dye/CuSCN photovoltaic cells, J. Phys. Chem. B **108**, 4342 (2004).
[22] B. C. O'Regan, S. Scully, A. C. Mayer, E. Palomares, and J. Durrant, The effect of Al_2O_3 Barrier Layers in TiO_2/dye/CuSCN photovoltaic cells explored by recombination and DOS characterization using transient photovoltage measurements, J. Phys. Chem. B **109**, 4616 (2005).
[23] B. C. O'Regan, J. R. Durrant, P. M. Sommeling, and N. J. Bakker, Influence of the $TiCl_4$ treatment on nanocrystalline TiO_2 films in dye-sensitized solar cells. 2. Charge density, band edge shifts, and quantification of recombination losses at short circuit, J. Phys. Chem. C **111**, 14001 (2007).
[24] S. A. Hawks, J. C. Aguirre, L. T. Schelhas, R. J. Thompson, R. C. Huber, A. S. Ferreira, G. Zhang, A. A. Herzing, S. H. Tolbert, and B. J. Schwartz, Comparing matched polymer: fullerene solar cells made by solution-sequential processing

and traditional blend casting: Nanoscale structure and device performance, J. Phys. Chem. C **118**, 17413 (2014).
[25] R. C. I. MacKenzie, C. G. Shuttle, M. L. Chabinyc, and J. Nelson, Extracting microscopic device parameters from transient photocurrent measurements of P3HT:PCBM solar cells, Adv. Energy Mater. **2**, 662 (2012).
[26] S. R. Cowan, R. A. Street, C. Shinuk, and A. J. Heeger, Transient photoconductivity in polymer bulk heterojunction solar cells: Competition between sweep-out and recombination, Phys. Rev. B **83**, 035205 (2011).
[27] R. A. Street, K. W. Song, J. E. Northrup, and S. Cowan, Photoconductivity measurements of the electronic structure of organic solar cells, Phys. Rev. B **83**, 165207 (2011).
[28] A. Pivrikas, N. S. Sariciftci, G. Juška, and R. Österbacka, A review of charge transport and recombination in polymer/fullerene organic solar cells, Prog. Photovoltaics **15**, 677 (2007).
[29] S. Albrecht, W. Schindler, J. Kurpiers, J. Kniepert, J. C. Blakesley, I. Dumsch, S. Allard, K. Fostiropoulos, U. Scherf, and D. Neher, On the field dependence of free charge carrier generation and recombination in blends of PCPDTBT/PC_{70}BM: Influence of solvent additives, J. Phys. Chem. Lett. **3**, 640 (2012).
[30] S. Bange, M. Schubert, and D. Neher, Charge mobility determination by current extraction under linear increasing voltages: Case of nonequilibrium charges and field-dependent mobilities, Phys. Rev. B **81**, 035209 (2010).
[31] R. A. Street, S. Cowan, and A. J. Heeger, Experimental test for geminate recombination applied to organic solar cells, Phys. Rev. B **82**, 121301(R) (2010).
[32] C. G. Shuttle, R. Hamilton, B. C. O'Regan, J. Nelson, and J. R. Durrant, Charge-density-based analysis of the current-voltage response of polythiophene/fullerene photovoltaic devices, Proc. Natl. Acad. Sci. U.S.A. **107**, 16448 (2010).
[33] T. Kirchartz, T. Agostinelli, M. Campoy-Quiles, W. Gong, and J. Nelson, Understanding the thickness-dependent performance of organic bulk heterojunction solar cells: The influence of mobility, lifetime, and space charge, J. Phys. Chem. Lett. **3**, 3470 (2012).
[34] S. A. Hawks, G. Li, Y. Yang, and R. A. Street, Band tail recombination in polymer:fullerene organic solar cells, J. Appl. Phys. **116**, 074503 (2014).
[35] D. Di Nuzzo, S. van Reenen, R. A. J. Janssen, M. Kemerink, and S. C. J. Meskers, Evidence for space-charge-limited conduction in organic photovoltaic cells at open-circuit conditions, Phys. Rev. B **87**, 085207 (2013).
[36] C. M. Proctor, M. Kuik, and T.-Q. Nguyen, Charge carrier recombination in organic solar cells, Prog. Polym. Sci. **38**, 1941 (2013).
[37] R. Hanfland, M. A. Fischer, W. Brutting, U. Wurfel, and R. C. I. MacKenzie, The physical meaning of charge extraction by linearly increasing voltage transients from organic solar cells, Appl. Phys. Lett. **103**, 063904 (2013).
[38] A. J. Morfa, A. M. Nardes, S. E. Shaheen, N. Kopidakis, and J. van de Lagemaat, Time-of-flight studies of electron-collection kinetics in polymer:fullerene bulk-heterojunction solar cells, Adv. Funct. Mater. **21**, 2580 (2011).
[39] G. Juška, K. Arlauskas, R. Österbacka, and H. Stubb, Time-of-flight measurements in thin films of regioregular poly(3-hexyl thiophene), Synth. Met. **109**, 173 (2000).
[40] R. A. Street, Measurements of depletion layers in hydrogenated amorphous silicon, Phys. Rev. B **27**, 4924 (1983).
[41] B. J. Tremolet de Villers, R. C. I. MacKenzie, J. J. Jasieniak, N. D. Treat, and M. L. Chabinyc, Linking vertical bulk-heterojunction composition and transient photocurrent dynamics in organic solar cells with solution-processed MoO_x contact layers, Adv. Energy Mater. **4**, 1301290 (2014).
[42] Z. Li, G. Lakhwani, N. C. Greenham, and C. R. McNeill, Voltage-dependent photocurrent transients of PTB7 : PC_{70}BM solar cells: Experiment and numerical simulation, J. Appl. Phys. **114**, 034502 (2013).
[43] G. Juška, K. Arlauskas, M. Viliunas, and J. Kocka, Extraction Current Transients: New Method of Study of Charge Transport in Microcrystalline Silicon, Phys. Rev. Lett. **84**, 4946 (2000).
[44] J. Lorrmann, B. H. Badada, O. Inganas, V. Dyakonov, and C. Deibel, Charge carrier extraction by linearly increasing voltage: Analytic framework and ambipolar transients, J. Appl. Phys. **108**, 113705 (2010).
[45] A. J. Mozer, N. S. Sariciftci, L. Lutsen, D. Vanderzande, R. Osterbacka, M. Westerling, and G. Juska, Charge transport and recombination in bulk heterojunction solar cells studied by the photoinduced charge extraction in linearly increasing voltage technique, Appl. Phys. Lett. **86**, 112104 (2005).
[46] B. T. D. Villers, C. J. Tassone, S. H. Tolbert, and B. J. Schwartz, Improving the reproducibility of P3HT:PCBM solar cells by controlling the PCBM/cathode interface, J. Phys. Chem. C **113**, 18978 (2009).
[47] G. Juška, N. Nekrašas, K. Genevičius, J. Stuchlik, and J. Kočka, Relaxation of photoexited charge carrier concentration and mobility in μc-Si : H, Thin Solid Films **451–452**, 290 (2004).
[48] N. Nekrašas, K. Genevičius, M. Vilinas, and G. Juška, Features of current transients of photogenerated charge carriers, extracted by linearly increased voltage, Chem. Phys. **404**, 56 (2012).
[49] See Supplemental Material at http://link.aps.org/supplemental/10.1103/PhysRevApplied.3.044014 for ancillary derivations and details on the drift-diffusion modeling.
[50] W. Shockley and W. Read, Jr., Statistics of the recombinations of holes and electrons, Phys. Rev. **87**, 835 (1952).
[51] R. N. Hall, Electron-hole recombination in germanium, Phys. Rev. **87**, 387 (1952).
[52] D. J. Griffiths, *Introduction to Electrodynamics*, 3rd ed. (Pearson, Upper Saddle River, NJ, 1999), pp. 73–74.
[53] K. Kawano, J. Sakai, M. Yahiro, and C. Adachi, Effect of solvent on fabrication of active layers in organic solar cells based on poly(3-hexylthiophene) and fullerene derivatives, Sol. Energy Mater. Sol. Cells **93**, 514 (2009).
[54] J. A. Carr and S. Chaudhary, The identification, characterization and mitigation of defect states in organic photovoltaic devices: A review and outlook, Energy Environ. Sci. **6**, 3414 (2013).
[55] S. Neugebauer, J. Rauh, C. Deibel, and V. Dyakonov, Investigation of electronic trap states in organic photovoltaic materials by current-based deep-level transient spectroscopy, Appl. Phys. Lett. **100**, 263304 (2012).

[56] J. Schafferhans, C. Deibel, and V. Dyakonov, Electronic trap states in methanofullerenes, Adv. Energy Mater. **1**, 655 (2011).
[57] R. A. Street, S. A. Hawks, P. P. Khlyabich, G. Li, B. J. Schwartz, B. C. Thompson, and Y. Yang, Electronic structure and transition energies in polymer-fullerene bulk heterojunctions, J. Phys. Chem. C **118**, 21873 (2014).
[58] S. R. Cowan, W. L. Leong, N. Banerji, G. Dennler, and A. J. Heeger, Identifying a threshold impurity level for organic solar cells: Enhanced first-order recombination via well-defined $PC_{84}BM$ traps in organic bulk heterojunction solar cells, Adv. Funct. Mater. **21**, 3083 (2011).
[59] S. Dongaonkar, J. D. Servaites, G. M. Ford, S. Loser, J. Moore, R. M. Gelfand, H. Mohseni, H. W. Hillhouse, R. Agrawal, M. A. Ratner, T. J. Marks, M. S. Lundstrom, and M. A. Alam, Universality of non-Ohmic shunt leakage in thin-film solar cells, J. Appl. Phys. **108**, 124509 (2010).
[60] T. Kirchartz, F. Deledalle, P. S. Tuladhar, J. R. Durrant, and J. Nelson, On the differences between dark and light ideality factor in polymer:fullerene solar cells, J. Phys. Chem. Lett. **4**, 2371 (2013).
[61] A. Wagenpfahl, C. Deibel, and V. Dyakonov, Organic solar cell efficiencies under the aspect of reduced surface recombination velocities, IEEE J. Sel. Top. Quantum Electron. **16**, 1759 (2010).
[62] T. Kirchartz, B. E. Pieters, K. Taretto, and U. Rau, Mobility dependent efficiencies of organic bulk heterojunction solar cells: Surface recombination and charge transfer state distribution, Phys. Rev. B **80**, 035334 (2009).
[63] J. C. Blakesley, F. A. Castro, W. Kylberg, G. F. Dibb, C. Arantes, R. Valaski, M. Cremona, J. S. Kim, and J.-S. Kim, Towards reliable charge-mobility benchmark measurements for organic semiconductors, Org. Electron. **15**, 1263 (2014).
[64] D. J. Griffiths, *Introduction to Electrodynamics*, 3rd ed. (Pearson, Upper Saddle River, NJ, 1999), pp. 96–98.
[65] W. Regan, S. Byrnes, W. Gannett, O. Ergen, O. Vazquez-Mena, F. Wang, and A. Zettl, Screening-engineered field-effect solar cells, Nano Lett. **12**, 4300 (2012).
[66] D. J. Griffiths, *Introduction to Electrodynamics*, 3rd ed. (Pearson, Upper Saddle River, NJ, 1999), p. 102.
[67] J. Bisquert and G. Garcia-Belmonte, On voltage, photovoltage, and photocurrent in bulk heterojunction organic solar cells, J. Phys. Chem. Lett. **2**, 1950 (2011).
[68] T. Walter, R. Herberholz, C. Müller, and H. W. Schock, Determination of defect distributions from admittance measurements and application to $Cu(In,Ga)Se_2$ based heterojunctions, J. Appl. Phys. **80**, 4411 (1996).
[69] J. Bisquert, Chemical capacitance of nanostructured semiconductors: Its origin and significance for nanocomposite solar cells, Phys. Chem. Chem. Phys. **5**, 5360 (2003).
[70] I. Mora-Seró, J. Bisquert, F. Fabregat-Santiago, G. Garcia-Belmonte, G. Zoppi, K. Durose, Y. Proskuryakov, I. Oja, A. Belaidi, T. Dittrich, R. Tena-Zaera, A. Katty, C. Lévy-Clément, V. Barrioz, and S. J. C. Irvine, Implications of the negative capacitance observed at forward bias in nanocomposite and polycrystalline solar cells, Nano Lett. **6**, 640 (2006).
[71] A. Maurano, C. G. Shuttle, R. Hamilton, A. M. Ballantyne, J. Nelson, W. Zhang, M. Heeney, and J. R. Durrant, Transient optoelectronic analysis of charge carrier losses in a selenophene/fullerene blend solar cell, J. Phys. Chem. C **115**, 5947 (2011).
[72] D. Credgington, F. C. Jamieson, B. Walker, T.-Q. Nguyen, and J. R. Durrant, Quantification of geminate and non-geminate recombination losses within a solution-processed small-molecule bulk heterojunction solar cell, Adv. Mater. **24**, 2135 (2012).
[73] O. J. Sandberg, M. Nyman, and R. Österbacka, Effect of Contacts in Organic Bulk Heterojunction Solar Cells, Phys. Rev. Applied **1**, 024003 (2014).
[74] C. G. Shuttle, A. Maurano, R. Hamilton, B. O'Regan, J. C. de Mello, and J. R. Durrant, Charge extraction analysis of charge carrier densities in a polythiophene/fullerene solar cell: Analysis of the origin of the device dark current, Appl. Phys. Lett. **93**, 183501 (2008).
[75] D. Credgington and Y. Kim, Analysis of recombination losses in a pentacene/C_{60} organic bilayer solar cell, J. Phys. Chem. Lett. **2**, 2759 (2011).
[76] C. G. Shuttle, B. O'Regan, A. M. Ballantyne, J. Nelson, D. D. C. Bradley, and J. R. Durrant, Bimolecular recombination losses in polythiophene:fullerene solar cells, Phys. Rev. B **78**, 113201 (2008).
[77] T. Kirchartz and J. Nelson, Meaning of reaction orders in polymer:fullerene solar cells, Phys. Rev. B **86**, 165201 (2012).
[78] S. A. Choulis, J. Nelson, Y. Kim, D. Poplavskyy, T. Kreouzis, J. R. Durrant, and D. D. C. Bradley, Investigation of transport properties in polymer/fullerene blends using time-of-flight photocurrent measurements, Appl. Phys. Lett. **83**, 3812 (2003).
[79] H. Scher and E. W. E. Montroll, Anomalous transit-time dispersion in amorphous solids, Phys. Rev. B **12**, 2455 (1975).
[80] O. J. Sandberg, M. Nyman, and R. Österbacka, Direct determination of doping concentration and built-in voltage from extraction current transients, Org. Electron. **15**, 3413 (2014).
[81] A. Armin, G. Juška, B. W. Philippa, P. L. Burn, P. Meredith, R. D. White, and A. Pivrikas, Doping-induced screening of the built-in-field in organic solar cells: Effect on charge transport and recombination, Adv. Energy Mater. **3**, 321 (2013).
[82] S. W. Kettlitz, J. Mescher, N. S. Christ, M. Nintz, S. Valouch, A. Colsmann, and U. Lemmer, Eliminating *RC*-effects in transient photocurrent measurements on organic photodiodes, IEEE Photonics Technol. Lett. **25**, 682 (2013).
[83] B. Y. Finck and B. J. Schwartz, Understanding the origin of the *S*-curve in conjugated polymer/fullerene photovoltaics from drift-diffusion simulations, Appl. Phys. Lett. **103**, 053306 (2013).
[84] G. Juška, N. Nekrašas, V. Valentinavičius, P. Meredith, and A. Pivrikas, Extraction of photogenerated charge carriers by linearly increasing voltage in the case of Langevin recombination, Phys. Rev. B **84**, 155202 (2011).
[85] M. P. Eng, P. R. F. Barnes, and J. R. Durrant, Concentration-dependent hole mobility and recombination coefficient in bulk heterojunctions determined from transient absorption spectroscopy, J. Phys. Chem. Lett. **1**, 3096 (2010).

[86] L. A. A. Pettersson, L. S. Roman, and O. Inganas, Modeling photocurrent action spectra of photovoltaic devices based on organic thin films, J. Appl. Phys. **86**, 487 (1999).

[87] G. F. Burkhard, E. T. Hoke, and M. D. McGehee, Accounting for interference, scattering, and electrode absorption to make accurate internal quantum efficiency measurements in organic and other thin solar cells, Adv. Mater. **22**, 3293 (2010).

[88] C. Deibel and A. Wagenpfahl, Comment on Interface state recombination in organic solar cells, Phys. Rev. B **82**, 207301 (2010).

[89] C. Deibel, A. Baumann, A. Wagenpfahl, and V. Dyakonov, Polaron recombination in pristine and annealed bulk heterojunction solar cells, Synth. Met. **159**, 2345 (2009).

[90] A. J. Mozer, G. Dennler, N. S. Sariciftci, M. Westerling, A. Pivrikas, R. Österbacka, and G. Juška, Time-dependent mobility and recombination of the photoinduced charge carriers in conjugated polymer/fullerene bulk heterojunction solar cells, Phys. Rev. B **72**, 035217 (2005).

[91] M. T. Neukom, N. A. Reinke, K. A. Brossi, and B. Ruhstaller, Transient photocurrent response of organic bulk heterojunction solar cells, Proc. SPIE Int. Soc. Opt. Eng. **7722**, 77220V (2010).

[92] A. Seemann, T. Sauermann, C. Lungenschmied, O. Armbruster, S. Bauer, H.-J. Egelhaaf, and J. Hauch, Reversible and irreversible degradation of organic solar cell performance by oxygen, Solar Energy **85**, 1238 (2011).